Postprint of: Kuryłowicz-Cudowska A., Haustein E., Isothermal Calorimetry and Compressive Strength Tests of Mortar Specimens for Determination of Apparent Activation Energy, JOURNAL OF MATERIALS IN CIVIL ENGINEERING, Vol. 33, iss. 4 (2021), pp. 1-14, DOI: 10.1061/(ASCE)MT.1943-5533.0003634.

Isothermal Calorimetry and Compressive Strength Tests of Mortar Specimens for Determination of Apparent Activation Energy

Aleksandra Kuryłowicz-Cudowska, Ph.D.[1]; and **Elzbieta Haustein**, Ph.D.[2]

[1]Assistant Professor, Department of Mechanics of Materials and Structures, Faculty of Civil and Environmental Engineering, Gdańsk University of Technology, Narutowicza 11/12,
80-233 Gdańsk, Poland, Email: aleksandra.kurylowicz-cudowska@pg.edu.pl

[2]Assistant Professor, Department of Mechanics of Materials and Structures, Faculty of Civil and Environmental Engineering, Gdańsk University of Technology, Narutowicza 11/12,
80-233 Gdańsk, Poland, Email: elzbieta.haustein@pg.edu.pl

Abstract

The hydration process of cementitious materials involves a thermally activated reaction that depends on the composition of the mixture and the curing temperature. The main parameter affecting the temperature variation of cast-in-place concrete is the apparent activation energy, which can be used for the efficient prediction of the temperature evolution and maturity index of hardening concrete. This paper discusses two methods to determine the activation energy of mortar specimens, whose mixture proportions are based on standards. The first approach is based on isothermal calorimetry measurements, and the second involves compression tests of mortar samples stored under four different temperature conditions. Mortar mixtures with ordinary portland cement and two rates of cement substitution with siliceous fly ash (10% and 20%) are investigated. The values of the activation energy obtained using the two approaches are compared. Finally, the effectiveness of different tests in determining the activation energy, and thus, maturity index is highlighted.

Author keywords: Apparent activation energy; Mortar specimens; Isothermal calorimetry; Mortar compressive strength; Maturity method; Fly ash; Cast-in-place concrete.

Introduction

The development of advanced technologies in different industries has promoted the use of modern technologies in civil engineering. Numerical simulations and in situ measurements allow the temperature and strength distribution in concrete structures to be predicted (Cervera et al. 2002; Martinelli et al. 2013; Chr´ościelewski et al.2016; Kuryłowicz-Cudowska 2019). The compressive strength of cast-in-place concrete is typically assessed via compression tests involving cylindrical or cubic specimens. The results of destructive tests of small samples (150/300-mm cylinders or 150-mm cubes) are often not representative because concrete used in real structures hardens under completely different conditions, implying various initial boundary conditions and a larger volume of concrete. Thus, in recent years, there has been an increasing interest in the estimation of concrete strength with respect to time, space, and the volume of the tested element. This applies not only to ordinary and high performance concrete but also to lightweight concrete structures (Soutsos et al. 2013; Kurpinska et al. 2019; Kurpinska and Kułak 2019). In accordance with this trend, the authors developed an augmentedmaturity method, which extends the research procedures described in the ASTM C1074 standard (ASTM 2019a) and uses a numerical finite-element analysis program. This new approach was implemented in the construction process of the largest (in termsof span length) extradosed European bridge built in Poland (Kuryłowicz-Cudowska 2019; Kuryłowicz-Cudowska et al. 2020). The scientific support allowed the post-tension dates to be determined for every segment of the bridge deck and allowed the constructions costs to be reduced. Currently, access to computationalsoftware allows materials and engineering problems to be solved in detail (Mariak et al. 2017; Miśkiewicz et al. 2019).

The monitoring of temperature evolution is useful for evaluating the mechanical properties of young concrete, in contrast to old concrete, which can be assessed according to selected mechanical, physical, and chemical properties (Ambroziak et al. 2019). In the application of the augmented maturity method, proper determination of the boundary conditions is difficult. An important parameter that significantly affects the temperature distribution in hardening concrete is the apparent activation energy. Fig. 1 presents the temperature evolutions in the middle of the concrete plate of a box girder of an extradosed bridge. The measured line indicates the measured value, and the other lines are related to the

prediction of the temperature development [described in detail by Kuryłowicz-Cudowska (2019)] for various values of the activation energy. The effect of activation energy on the concrete temperature is clearly observed. Several studies have investigated the activation energy (Jonasson et al. 1994; Schindler 2004), which according to many researchers depends on the temperature, cement type, and mineral additions. Brooks et al. (2007) examined mortar cubes made of Type I cement and various replacement levels of fly ash (FA). The authors reported that the values of the activation energy ranged between 38.3 and 42.3 kJ=mol, and the strength–age relationship significantly affected the activation energy based on ASTM C1074 (ASTM 2019a). Poole et al. (2011) considered the effects of chemical admixtures on the value of the apparent activation energy. The authors reported that water-reducing admixtures reduced the activation energy and a vinsol resin air-entraining agent had no effect. Saadoon et al. (2019) developed new models based on the composition of the cement, curing temperature, fineness of cement, and water-to-cement ratio.

To increase the accuracy of the estimated strength, it is necessary to properly define the activation energy for the type of concrete under investigation. Thus, the main objective of this study was to examine the two methods for determining the activation energy of mortar, with a focus on the application of the maturity method to construction sites. The first and more recently proposed approach involves isothermal microcalorimetry measurements of the heat production in the mortar specimens. The second approach involves destructive compression tests of 50-mm mortar cubes stored at constant temperatures. Three types of mortar mixtures and four different curing temperatures were investigated. The tests results indicated the advantages and disadvantages of the two methods and allowed for the selection of the most appropriate research method.

Theoretical Background

Concrete maturity is directly related to time and temperature, which have an impact on the kinetics of concrete curing. ASTM C1074 (ASTM 2019a) describes two functions for calculating the maturity index. The recommended one is the maturity function, which gives the equivalent age t_e at a specified temperature T_s

$$t_e = \sum_0^t \exp\left(\frac{E_a}{R} \cdot \left(\frac{1}{T_s} - \frac{1}{T}\right)\right) \cdot \Delta t \tag{1}$$

where T = absolute concrete temperature; Δt = the time interval; R = 8.314 J/(mol·K) represents the gas constant; and E_a = apparent activation energy, which is the parameter to be determined. The thermally activated nature of hydration reactions was the main focus of this study.

Heat Generation of Cementitious Materials

Using isothermal calorimetry, the heat generation rate $\dot{Q}$ and corresponding accumulated heat of hydration Q can be measured for different cementitious materials. To characterize the advancement of the reaction, Azenha (2009) defined the degree of heat development α. This parameter is the ratio between the heat released until time t to the total accumulated heat Q_{tot}

$$\alpha = Q(t) / Q_{tot} \tag{2}$$

Time differentiation yields

$$\dot{\alpha} = \dot{Q}(t) / Q_{tot} \tag{3}$$

The asymptotic value Q_{tot} can be calculated by plotting $Q(1/t)$ and using nonlinear approximation for measurement data obtained after 50 h of the experiment $(1/t = 1/50 = 0.02)$. For $1/t \sim 0$, $g(\sim 0) = Q_{tot}$. One of the recommended fitting functions is

$$g\left(\frac{1}{t}\right) = a \exp\left(b \cdot \frac{1}{t}\right) \tag{4}$$

This approach was demonstrated by Azenha (2009) and Azenha et al. (2011). The detection of the first peak of the heat generation rate $\dot{Q}_{peak\_1}$, which occurs after a local minimum, allows the normalized heat generation rate to be determined as a function of the degree of heat development

$$f(\alpha) = \dot{Q}(\alpha) / \dot{Q}_{peak\_1} \tag{5}$$

The heat generation rate should be described using the Arrhenius equation

$$\dot{Q}(t) = f(\alpha) A \exp\left(\frac{-E_a}{RT}\right) \tag{6}$$

where R = gas constant; A = a rate constant; and E_a = apparent activation energy.

In this study, two methods described by Kada-benameur et al. (2000), D'Aloia and Chanvillard (2002), and Azenha (2009) were used to determine the activation energy. The first method is based on the relationship between the heat generation rates for two temperatures T_1 and T_2 of isothermal curing. Taking into account Eqs. (3) and (6), we obtain

$$\dot{\alpha} = \frac{f(\alpha) A}{Q_{tot}} \exp\left(\frac{-E_a}{RT}\right) \tag{7}$$

Assuming a fixed degree of heat development α_{ref}, the hydration rates for two calorimetric tests performed at distinct temperatures are expressed by the following equations

$$\begin{aligned} \left[\dot{\alpha}\left(\alpha_{ref}\right)\right]_{T_1} &= \frac{f(\alpha_{ref}) A}{Q_{tot}} \exp\left(\frac{-E_a}{RT_1}\right) \\ \left[\dot{\alpha}\left(\alpha_{ref}\right)\right]_{T_2} &= \frac{f(\alpha_{ref}) A}{Q_{tot}} \exp\left(\frac{-E_a}{RT_2}\right) \end{aligned} . \tag{8}$$

The ratio of these two formulas is the basis of the calculation of the apparent activation energy

$$E_a\left(\alpha_{ref}\right)\Big|_{T_2}^{T_1} = \frac{R(T_1 \cdot T_2)}{T_1 - T_2} \ln\left(\frac{\left[\dot{\alpha}\left(\alpha_{ref}\right)\right]_{T_1}}{\left[\dot{\alpha}\left(\alpha_{ref}\right)\right]_{T_2}}\right) \tag{9}$$

The second approach was described by Azenha (2009) and is recommended by ASTM C1074 (ASTM 2019a). With the logarithmic form of Eq. (6)

$$\ln\left(\dot{Q}_{Ti}\left(\alpha_{ref}\right)\right)=\ln\left(f(\alpha_{ref})A\exp\left(\frac{-E_a}{RT_i}\right)\right) \tag{10}$$

for each (i) isothermal calorimetry test, it is possible to use linear function $Y=n\cdot X+p$ to determine both E_a and A. By letting the X-axis indicates the reciprocal of the absolute temperature $1/T_i$ and the Y-axis indicates $\ln\left(\dot{Q}_{Ti}\left(\alpha_{ref}\right)\right)$, the values of $n=-E_a/R$ and $p=\ln\left(f(\alpha_{ref})A\right)$ can be obtained. If the foregoing procedure is repeated for individual degrees of heat development, the relationship between E_a and α_{ref} can be plotted, generally for the whole period between $\alpha_{ref}=0$ and $\alpha_{ref}=1$. Nevertheless, Wadsö (2003) and Azenha (2009) recommended analyzing the degree of heat development conforming to the peak value $\dot{Q}_{peak\_1}$, because the first maximum of the heat generation rate occurs at approximately the same degree of heat development for every considered temperature in isothermal calorimetry. Thus, a specified, unique value of E_a is the most representative in the whole hydration process.

Compressive Strength Under Isothermal Conditions

A similar relationship between the natural logarithm of the heat generation rate and the reciprocal of the temperature is discussed in the annex of ASTM C1074 (ASTM 2019a). However, the difference lies in the method of analyzing the specimens. Considering the aforementioned standard (ASTM 2019a), studies on 50-mm mortar cubes cured at constant temperatures in water baths are performed. The proportion of mortar mixture corresponds to the recipe of cast-in-place concrete. Considering this, the compressive-strength data of mortar cubes are the basis of future calculations.

The annex of ASTM C1074 (ASTM 2019a) provides three methods for determining the apparent activation energy E_a. Mariak et al. (2018) analyzed all of them in detail. The procedures described in points A.1.1.7 and A.1.1.8.2 of ASTM C1074 (ASTM 2019a) include linear regression analysis of the reciprocal of the age versus the reciprocal of the average cubic strength. Because the development of the early-age strength of mortar is highly nonlinear, linear approximation does not provide the desired results and, thus, it is not recommended. The proper solution method is based on the computational

approximation of strength-age data to define rate constants ($k-$values) by fitting the set of data with a nonlinear equation. One of the functions that has been included in A1.1.8.1 of ASTM C1074 (ASTM 2019a) is the hyperbolic formulation

$$S = S_u \cdot \frac{k \cdot (t - t_0)}{1 + k \cdot (t - t_0)} \tag{11}$$

where S = compressive strength at time t; S_u = ultimate compressive strength; and t_0 = age at which the strength development begins. The parameters S_u, k, and t_0 are determined via least-squares regression. The second, stretched exponential (with beta as the stretching coefficient) function proposed by Freiesleben Hansen and Pedersen (1985) is given as follows:

$$S = S_u \cdot \exp\left(-\left[\frac{\tau}{t}\right]^{\beta}\right) \tag{12}$$

where τ = a time constant; and β = a shape constant.

Knowledge of the $k-$values allows the natural logarithm of these values to be plotted with respect to the reciprocal of the temperature (in kelvins). The slope of the best-fit straight line is the activation energy E_a divided by the gas constant R.

Materials and Testing Methodology

Laboratory tests were performed using ordinary portland cement (OPC) CEM I 42.5 R (CEN 2000) supplied from Cement Company Górażdże (Gdynia, Poland) and FA obtained from a thermal power plant (Power Station Opole, Brzezie, Poland). The chemical compositions (oxides) of the portland cement and FA were determined via X-ray fluorescence spectroscopy (RS3400, Bruker AXS Corporation, Karlsruhe, Germany) and quantitative X-ray diffraction analysis, and the results are presented in Table 1.

The morphology of the FA was examined using a scanning electron microscope (Microscope type XL30, Philips, Electron optics Company, Eindhoven, Netherlands), as shown in Fig. 2. A large portion of the FA particles were spherical. The relatively small FA particles had a compact smooth wall surface and closed pores. The large grains had irregular shapes and a deformed surface structure with open

visible pores. The variety of morphological changes in FA is related to the temperature changes during the combustion of coal (Haustein and Kuryłowicz-Cudowska 2020). It was also suggested (Vu et al. 2019, Kleinhans et al.2018) that the FA particles depend on the temperature of combustion of coal and the transformation of intrinsic mineral matter (e.g., in the form of solid, irregular shapes and hollow spherical particles or the deformed surface of their structure). To determine the effect of the ash grain size (including its shape) on the heat of the hydration process, more advanced studies must be performed.

The ASTM C618 standard (ASTM 2019b) provides chemical and physical criteria related to the classification of FA, as given in Table 2. According to this classification, the FA used in the present study belonged to the F Class. Primarily oxides were detected in FA: SiO_2, Al_2O_3, and Fe_2O_3. These oxides are typically present in the form of an amorphous (glassy) phase that causes pozzolanic activity of FA during hydration with cement. At early ages of hydration, FA particles often act as microaggregates, filling the pores of binders and nuclei of the hydration products, whereas at later ages, the chemical effect of FA is observed. FA can react with $Ca(OH)_2$, which is a product of cement hydration that forms C–S–H gel. This is the pozzolanic reaction, which in the case of FA is significantly slower than the hydration of cement (Feng et al. 2018).

The composition of 1 m^3 of the considered concrete was as follows: cement, 440 kg; water, 175 kg; siliceous sand 0/2, 700 kg; basalt aggregates 2/8, 534 kg; and basalt aggregates 8/16, 608 kg. According to the concrete composition, mortar specimens were fabricated. Proportions of mortar mixtures were based on A1.1.2 of the ASTM C 1074 standard (ASTM 2019a). Thus, the fine aggregate-to-cement ratio of the mortar mixture was identical to the coarse aggregate-to-cement ratio of the concrete mixture under investigation. The mixture had also the same water-to-cementitious materials ratio as the concrete. Additionally, to extend this research, two substitution rates of OPC with siliceous FA were considered: 10% and 20%. In all three cases, the water-to-binder ratio of the cement mortars was 0.4. The experimental program comprised calorimetric and compression strength tests for three mortar compositions with curing at four temperatures: 23°C, 33°C, 43°C, and 53°C.

Isothermal calorimetry is used to analyze the time development of the hydration heat (J/g) and heat evolution rate [J/(g·h)] of cementitious materials. Isothermal refers to the constant temperature aspect of the test. The advantage of this method is the high precision of the measurement instrument compared

with semiadiabatic and adiabatic devices. In the present study, the heat flow of mortar hydration was measured using a TAM Air three-channel isothermal calorimeter (TA Instruments, New Castle, Delaware) [Fig. 3(a)], which conformed to two ASTM standards associated with cement: ASTM C1702 (ASTM 2017b) and ASTM C1679 (ASTM 2017a). The device was designed for heat measurements of large-volume paste, mortar, or concrete specimens [0.000125 m^3 (125 mL) glass ampoule, Fig. 3b)]. Many scientists conduct research using paste specimens, but according to ASTM C1679 (ASTM 2017a), mortar samples may provide results that have better correlation with concrete setting and early strength development, which was the focus of this study. During each test, the measurements were recorded continuously over 7 days by a three-channel data logger, which was connected to a computer. The baseline was measured for a minimum of 12 h to achieve signal stability conditions using a linear least-squares procedure (the absolute value of the slope of the calorimetric signal was <3 μW/h, and the standard deviation was <12 μW). For each test, six ampoules (three samples and three reference ampoules) were prepared. The sample and reference ampoules were balanced; that is, they had the same thermal response, to ensure a stable baseline. This was achieved by using an inert material with approximately the same heat capacity as the sample in the reference ampoules.

The mortar cubes were molded in accordance with ASTM C109/C109M (ASTM 2016) and then cured under isothermal conditions [i.e., in controlled-temperature water baths (Fig. 4)]. Before the destructive tests, the specimens were removed from the baths and wiped to surface-dry conditions. Any loose sand grains that would have been in contact with the testing machine were removed. The load rate of the specimens, which was expressed as the movement between the upper and lower platens, was 1,000 N/s. Compression tests were performed on three 50-mm mortar cubes from each mixture at 6 or 12 h and 1, 2, 5, 7, and 14 days. All the specimens for a given test age were broken within the tolerance permissible in ASTM C109/C109M (ASTM 2016). A total number of prepared mortar samples was 216 (3 mixtures × 4 temperatures × 18 cubes per mixture).

Experimental Results and Discussion

Isothermal Calorimetry

Generally, the cement hydration process can be divided into five steps: the rapid initial process, induction, acceleration, retardation, and slow continued reaction period (Klemczak and Batog 2016). The amount of supplementary cementitious materials (SCM) and curing conditions significantly affect the rate and heat of hydration. The effects of FA addition and the curing temperature on the evolution of the mortar hydration are presented in Fig. 5 and Fig. 6, respectively. In Fig. 5, the heat measurements performed at 23°C and 43°C are indicated by solid lines, and those performed at 33°C and 53°C are indicated by dotted lines. For clarity, the graphs depict the first 48 h of the heat generation rate.

As shown in Fig. 5, the heat released from the examined mortars and the main hydration peak decreased significantly with the increasing amount of added minerals, owing to the lower rate of the pozzolanic reaction of FA. FA addition reduced the hydration rate regardless of the curing temperature; it slightly delayed the occurrence of the hydration peak and significantly reduced the peak value. In every considered condition, mineral addition reduced the total amount of the heat released during the hydration process [Figs. 5(b and d)].

The total (at 165 h) heat emission of mortar containing 10% and 20% FA decreased by 10.4% and 16.8%, respectively, at 23°C [Fig. 5(b)] and by 10.0% and 9.7%, respectively, at 53°C [Fig. 5(d)] compared with the mortar without mineral addition. Moghaddam et al. (2019) reported that the cumulative heat of hydration generated for cement samples with FA was lower than that for samples without FA. Snelson et al. (2008) noted that the small specific surface area and low solubility of the aluminosilicate present in the FA are the main factors contributing to the reduction in the total amount of heat released. At high temperatures (≥33°C), for the mixtures with FA, there were slight differences in the total amount of heat released at 165 h [Figs. 5(b and d)], owing to the small modifications in the amount of FA. Additionally, with the increasing mass of cement substitution, the induction period of hydration was prolonged [Figs. 5(a and c)], but when the curing temperature increased from 23°C to 53°C, the induction period was shortened [Figs. 6(a, c, and e)].

As shown in Figs. 6(a, c, and e), increasing the temperature accelerated the hydration reaction and led to higher rates of heat evolution from the mortar, confirming the thermally activated nature of the hydration reaction. Increasing the curing temperature increased the value of the hydration peak and the total amount of heat, for both the OPC mortar mixture and mixtures with different substitution rates of FA (Fig. 6). The heat released at 12 h for OPC, and the 10% and 20% FA mortar mixtures was 2.9, 3.1, and 3.5 times higher at 53°C compared with the data measured at 23°C [Figs. 6(b, d, and f)]. The profiles of the heat flow indicated that at 23°C and 33°C, the second exothermic peak was lower than the first one, whereas at 43°C and 53°C, the second peak was higher. Additionally, at 53°C, the second peak was very narrow, and its value increased significantly [Figs. 6(a, c, and e)]. Klemczak and Batog (2016) reported similar observations regarding the second peak. The second peak indicates a renewal reaction of C_3A with the depletion of gypsum. Additionally, the substitution of cement with FA reduces the gypsum content and increases the reactivity of C_3A (Moghaddam et al. 2019).

It was previously reported (Feng et al. 2018; Deschner et al. 2012) that in the process of hydration, the precipitation of the CSH and $Ca(OH)_2$ phases requires the saturation of the Ca^{2+} concentration in the liquid phase of the cement mortar. When some part of the cement is replaced by FA of F Class, the Ca^{2+} is adsorbed on the surfaces of FA particles. Reducing the cement content in the mortar specimen reduces the Ca^{2+} concentration in the liquid phase, delaying the saturation of Ca^{2+}. Therefore, the increased content of FA in the cement mortar delays the early-age hydration and the appearance of the second exothermic peak [Figs. 5(a and c)].

Mortar Compression Tests

Compression tests were performed on cubes stored at 33°C, 43°C, and 53°C for 6 h and 1, 2, 5, 7, and 14 days, and on samples cured at 23°C for 12 h and 1, 2, 5, 7, and 14 days. The reason was the effect of the high curing temperature on the strength gain. The time evolutions of the average compressive strength for 50-mm mortar cubes are shown in Fig. 7. The standard deviation of the strength (SSD) for every three mortar cubes varied between 0.1 and 5.3 MPa. The average SSD for all the cubes made of mortar with OPC was 1.1 MPa, and those for the cubes made of mortar with 10% and 20% FA were 1.6 and 1.4 MPa, respectively.

The temperature of the water bath significantly affected the strength development. For all the considered mortar mixtures, the early-age strength increased with the curing temperature. After 6 h of hardening, the strengths of the mortar cubes cured at 33°C and 53°C were 4 MPa [Fig. 7(b)] and approximately 19 MPa [Fig. 7(d)], respectively. The largest difference in the strength evolution was observed for the specimens stored at 23°C. The addition of 20% FA reduced the 14-days strength by 29.5% compared with cubes without any supplementary materials [Fig. 7(a)]. For the other curing temperatures, there were no visible strength differences after 14 days. However, the strength changes presented in Figs. 7(a–d) indicate that the addition of FA reduced the strength (the pozzolanic reaction was slower than the cement hydration rate) for a low curing temperature (23°C) and increased the strength for a high curing temperature (53°C) compared with the control cement mortar devoid of FA. Therefore, the substitution of cement with FA can enhance the long-term compressive strength, particularly in the core of heavy- and medium-weight structures, wherein high concrete temperatures frequently occur. The OPC samples subjected to high temperatures at early ages exhibited higher early-age compressive strengths but lower later-age strengths than cubes subjected to normal temperatures (Kim et al. 2002).

Determination of Apparent Activation Energy

Calculations Using Calorimetric Tests

With reference to the data obtained via isothermal colorimetric measurements, two methods to determine the activation energy were examined. The calculations were performed in MATLAB version R2017b.

First Approach

To calculate the total accumulated heat Q_{tot}, nonlinear regression of Eq. (4) using least-squares method was performed. For every mortar mixture, the relationship between the hydration heat and the reciprocal of time $[Q(1/t)]$ was plotted, but only the data obtained after 50 h of the experiment $(1/t < 0.02)$ were used. The results of the extrapolation procedure for the mortar mixture with OPC are shown in Fig. 8.

For the three analyzed mortar types, the coefficient of determination (R^2) was within the range of 0.9827–0.9996 (Table 3).

The degree of heat development α was calculated for every recipe, but only the results for mortar with OPC are presented in Fig. 9. This relationship allowed the heat generation rate $\dot{Q}$ to be plotted with respect to α (Fig. 10a). All the graphs exhibited a similar shape, and the first peak occurred at the same value of $\alpha \approx 0.2$. By dividing the rate of heat evolution $\dot{Q}$ by the first peak of the heat generation rate $\dot{Q}_{peak\_1}$, the normalized heat generation rate $f(\alpha)$ was obtained, as shown in Fig. 10(b). The obtained curves for every curing temperature were coincident at $\alpha \approx 0.2$. The same situation was observed for the second peak at $\alpha \approx 0.4$.

The main values of the heat evolution for the considered mortars are presented in Table 4. The extrapolated amounts of the total heat tended to increase with the curing temperature. The same trend was observed for the peak value $\dot{Q}_{peak\_1}$. For the mortar with OPC, when the curing temperature increased by 30 °C, the amount of time taken for the peak to occur decreased by a factor of 3: from 10.5 to 3.5 h (Table 4). The mortar specimens containing 20% FA exhibited the lowest total heat in all cases. One parameter [i.e., $\alpha(\dot{Q}_{peak\_1})$], was independent of the mortar type and curing temperature and remained almost constant (it varied from 0.18 to 0.24).

According to the data provided by the isothermal measurements performed at two different temperatures and the fixed value of the degree of heat development α_{ref}, the apparent activation energy was calculated using Eq. (9). At the beginning of the hydration reaction, rapid heat evolution caused by the formation of an amorphous layer of hydration product around the cement particles was observed; thus, the activation energy E_a was calculated for $\alpha_{ref} \geq 0.1$.

In the three temperature intervals of 23°C–33°C, 33°C–43°C, and 43°C–53°C [Figs. 11(a-c)], the apparent activation energy exhibited large variations with respect to the degree of heat development, particularly for $\alpha_{ref} > 0.4$, regardless of the mortar type. The smallest variations in E_a were observed for the mortar with OPC [Fig. 11(a)]. For α_{ref} between 0.15 to 0.40, in the three temperature ranges, the average value of the activation energy for mortar with OPC, OPC + 10% FA, and OPC + 20% FA was

44.190, 41.067, and 39.700 kJ/mol, respectively. The results indicate that the addition of FA reduced the apparent activation energy. Cement substitution with 10% and 20% FA reduced E_a by 7.1% and 10.2%, respectively, compared with the mortar with OPC.

In the temperature ranges of 23°C–43°C and 33°C–53°C [Figs. 11(d-f)], the oscillations of E_a were slightly smaller than in the three temperature intervals. In the interval of 33°C–53°C, the activation energy decreased for α_{ref} values higher than 0.38 [Fig. 11(d)], 0.33 [Fig. 11(e)], and 0.31 [Fig. 11(f)]. The average value of E_a for $\alpha_{ref} \in \langle 0.15, 0.40 \rangle$ in the two aforementioned temperature ranges was 46.880, 45.425, and 39.575 kJ/mol for mortar with OPC, OPC + 10% FA, and OPC + 20% FA, respectively. The addition of 10% and 20% FA reduced the activation energy by 3.1% and 15.6%, respectively, compared with the mortar without mineral addition. For $\alpha_{ref} = 0.2$, in the two temperature intervals, the average value of E_a for the three aforementioned mortar mixtures was 45.750, 43.085, and 39.200 kJ/mol, respectively (for the mortar with OPC, the temperature range of 33°C–53°C was disregarded).

Although trends were observed in the evolution of the activation energy, the variations of this parameter were considerable. As shown in Fig. 11, the average value of E_a oscillated around a value of 39–45 kJ/mol, where the upper limit corresponds to the OPC mortar and the lower one corresponds to the mortar with 20% FA. Thus, the described method for the determination of the apparent activation energy provided good results that could be applied to the equivalent age Eq. (1) of the maturity method for the estimation of the strength of cast-in-place concrete.

Second Approach

If one focuses on the rate of heat evolution, the logarithmic Eq. (10) can be used. According to the results in Fig. 10(a) and Table 4, the first exothermic peak $\dot{Q}_{peak\_1}$ occurred at the same degree of heat development $\alpha \approx 0.2$ for all the considered mortar mixtures. Thus, the relationships of $\ln\left(\dot{Q}_{peak\_1}\right)$ versus the reciprocal of the absolute curing temperature $1/T$ were plotted, as shown in Fig. 12. The dots indicate the results of four isothermal tests, and the lines indicate the results of linear approximations

using the least-squares method. The computed value of the apparent activation energy for mortar with OPC was 41.557 kJ/mol. With the replacement of 10% and 20% OPC with FA, values of 40.934 and 39.961 kJ/mol were obtained. For the mortars with FA addition, the value of E_a was reduced by 1.5% and 3.8%, respectively, compared with that for the OPC mixture. Thus, the results obtained using this approach differed slightly from each other, compared with the activation-energy values given in first approach.

Further calculations were performed to verify other values of the heat development degree. The linear regressions for $\alpha_{ref} \in \langle 0.2 : 0.1 : 0.8 \rangle$ are shown in Fig. 13(a). The same procedure was repeated for the whole spectrum of α_{ref}. Clearly, for all the investigated compositions, the activation energy increased for $\alpha_{ref} < 0.32 - 0.38$ and then decreased with the advancement of the hydration reaction. For α = 0.2, E_a was constant, confirming the advantages and importance of the first exothermic peak of the heat generation rate.

Calculations Using Mechanical Tests

The strength–age relationships for the mortar cubes in Fig. 14 were computed using the exponential Eq. (12) discussed in the section "Theoretical Background". When mortar with OPC and OPC + 10% FA were considered, the crossover effect for a curing temperature of 53 °C occurred at the ages of 33 and 49 h, respectively, and there were reductions of 30% and 20%, respectively, in the 14-days strength compared with the mortar cured at 23 °C. When 20% of the cement mass was replaced by FA, the crossover effect was not observed.

A detailed analysis of the least-squares regression of the strength–age data using Eq. (11) and (12) and the apparent activation energy are presented in Tables 5 and 6. The determination coefficient for the nonlinear analysis of the strength development was >0.9196 for all the cases. The rate constants (k) were similar for the two analyzed functions, but the value of the activation energy differed significantly. According to the hyperbolic function, the value of E_a for the mortar with OPC was 41.077 kJ/mol, and for the mortar containing 10% and 20% FA, E_a was reduced to 35.020 and 33.975 kJ/mol, respectively

(reductions of 14.7% and 17.3%). In the case of exponential regression, the E_a values were higher. As shown in Fig. 14, a linear relationship correctly characterized the data in the Arrhenius plot. When only cement was used, E_a was 44.011 kJ/mol. When 10% and 20% mass of cement was replaced by FA, E_a decreased to 39.986 and 37.686 kJ/mol, respectively. Compared with the OPC mixture, the E_a values for the mortar with FA were reduced by 9.1% and 14.4%. The experimental results confirmed that siliceous FA addition reduces E_a; nevertheless, the choice of the function significantly influences the determined value of the apparent activation energy.

According to the plot for the strength-maturity relationship at 23°C, the mortar compressive strengths with curing temperatures of 33°C, 43°C and 53°C were predicted (Fig. 15). The calculations were performed using the exponential function Eq. (12) expressed in equivalent age (1), including the value of E_a from Table 6. For the mortar with OPC [Fig. 15(a)] and OPC + 10% FA [Fig. 15(b)], the strength was overestimated, particularly for the mortars cured at 53°C. This was due to the assumptions of the maturity method [i.e., that increasing the temperature increases the maturity index (equivalent age) and the strength]. As shown in Figs. 14(a and c), the strengths of the specimens cured at elevated temperatures after 2 days were reduced compared with those of the samples cured at 23°C. The classical maturity method does not consider the crossover effect (Kjellsen and Detwiler 1993). For the mortar containing 20% FA [Fig. 15(c)], the strengths were close to the 45° line, with an error range of <20%. As shown in Figs. 5 and 6, the addition of FA reduced the hydration process, resulting in a smaller strength gain and smaller strength differences [Fig. 14(e)] compared with the mortars with OPC and OPC + 10% FA [Figs. 14(a and c)]. In this case [Fig. 14(e)], the crossover effect was not observed. This is why the mineral addition positively influenced the strength development at high curing temperatures.

Conclusions

This study focused on identifying the most reliable way to determine the apparent activation energy of mortar specimens. The specific value of E_a required for implementation of the maturity function corresponds to the advancement of the hydration reaction through an equivalent age. The accurate prediction of the concrete temperature and compressive-strength evolution depends primarily on the

value of the apparent activation energy. Therefore, with regard to two independent methods—calorimetric and mechanical tests—the following conclusions are drawn:

- For both methods, the addition of siliceous FA reduced the hydration rate and thus decreases the apparent activation energy of the mortar specimens.
- In the first approach (calorimetric tests), owing to the variations in E_a, the analysis provided reliable results for degrees of heat development in the range of <0.4. In the second (logarithmic) approach, the calculations of E_a should be performed for the first exothermic peak, because it occurs at the same value of α, regardless of the curing temperature.
- According to the four different scopes of analysis for calorimetric results, the values of E_a for mortar with OPC were 44.190, 46.880, 45.750, and 41.557; those for mortar with 10% FA were 41.067, 45.425, 43.085, and 40.935; and those for mortar with 20% FA were 39.700, 39.575, 39.200, and 39.961. The same trend in E_a was observed for the three mixtures. The average of the foregoing activation energy values for the three considered mixtures (OPC, OPC + 10% FA, and OPC + 20% FA) was 44.6, 42.6, and 39.6 kJ/mol, respectively. The addition of 10% and 20% SCM reduced the activation energy by 4.5% and 11.2%, respectively.
- The activation energy determined in compressive strength tests of mortar specimens depended on the approximation equation and the results obtained in this way were different. For mortar without FA and with 10% and 20% FA, in the case of hyperbolic regression, E_a was 41.077, 35.020, and 33.975 kJ/mol, respectively, and in relation to an exponential function, E_a was 44.011, 39.986, and 37.686 kJ/mol, respectively. Thus, despite the same strength–age data, uncertain results were achieved. The advantages of proposed equations cannot be clearly identified. The ASTM C1074 standard uses the hyperbolic function, but many researchers use both formulations. However, the activation energy values obtained using the exponential equation were more consistent with the results of the calorimetric approach in this study.

- The discussed regression functions include three approximated parameters. To increase the curve-fitting accuracy, it is recommended to determine one constant (e.g. the ultimate compressive strength) experimentally in compression tests at an age of 28 (or better, 56-days).
- Isothermal calorimetry is an extremely precise technique; thus, except during the preparation of the mortar specimens, the heat flow is measured with a sensitivity in the microwatt range, which ensures the stability and repeatability of the test results.
- Calorimetry tests can take <7 days, (e.g., 3 days), because after 72 h, the degree of heat development is >0.8, and the first peak of the heat generation rate generally occurs within the first 12 h.
- The results obtained via the calorimetric method were more consistent than those of the compression tests. In general, both the calorimetric and mechanical methods are useful. However, calorimetry tests are strongly recommended.

References

Ambroziak, A., E. Haustein, and J. Kondrat. 2019. "Chemical and mechanical properties of 70-year-old concrete." *J. Mater. Civ. Eng.* 31 (8): 04019159. https://doi.org/10.1061/(ASCE)MT.1943-5533.0002840.

ASTM. 2016. *Standard test method for compressive strength of hydraulic cement mortars [Using 2-in. or (50-mm) cube specimens]*. ASTM C109/C109M. West Conshohocken, PA: ASTM.

ASTM. 2017a. *Standard practice for measuring hydration kinetics of hydraulic cementitious mixtures using isothermal calorimetry.* ASTM C1679. West Conshohocken, PA: ASTM.

ASTM. 2017b. *Standard test method for measurement of heat of hydration of hydraulic cementitious materials using isothermal conduction calorimetry.* ASTM C1702. West Conshohocken, PA: ASTM.

ASTM. 2019a. *Standard practice for estimating concrete strength by the maturity method.* ASTM C1074. West Conshohocken, PA: ASTM.

ASTM. 2019b. *Standard specification for coal fly ash and raw or calcined natural pozzolan for use in concrete.* ASTM C618. West Conshohocken, PA: ASTM.

Azenha, M. 2009. "Numerical simulation of the structural behaviour of concrete since its early ages." Ph.D. thesis, Faculty of Engineering, Univ. of Porto.

Azenha, M., C. Sousa, R. Faria, and A. Neves. 2011. "Thermo–hygro– mechanical modelling of self-induced stresses during the service life of RC structures." *Eng. Struct.* 33 (Dec): 3442–3453. https://doi.org/10.1016/j.engstruct.2011.07.008.

Brooks, A. G., A. K. Schindler, and R.W. Barnes. 2007. "Maturity method evaluated for various cementitious materials." *J. Mater. Civ. Eng.* 19 (12): 1017–1025. https://doi.org/10.1061/(ASCE)0899-1561(2007) 19:12(1017).

CEN (European Committee for Standardization). 2000. *Cement—Part 1: Compositions, specifications ad conformity criteria for common cements*. EN 197-1. Brussels, Belgium: CEN.

Cervera, M., R. Faria, J. Oliver, and T. Prato. 2002. "Numerical modelling of concrete curing, regarding hydration and temperature phenomena." *Comput. Struct.* 80 (18–19): 1511–1521. https://doi.org/10.1016/S0045-7949(02)00104-9.

Chróścielewski, J., A. Mariak, A. Sabik, B. Meronk, and K. Wilde. 2016. "Monitoring of concrete curing in extradosed bridge supported by numerical simulation." *Adv. Sci. Technol. Res. J.* 10 (32): 254–262. https://doi.org/10.12913/22998624/66186.

D'Aloia, L., and G. Chanvillard. 2002. "Determining the 'apparent' activation energy of concrete: E_a—numerical simulations of the heat of hydration of cement." *Cem. Concr. Res.* 32 (8): 1277–1289. https://doi .org/10.1016/S0008-8846(02)00791-3.

Deschner, F., F. Winnefeld, and B. Lothenbach. 2012. "Hydration of a Portland cement with high replacement by siliceous fly ash." *Cem. Concr. Res.* 42 (10): 1389–1400. https://doi.org/10.1016/j.cemconres .2012.06.009.

Feng, J., J. Sun, and P. Yan. 2018. "The influence of ground fly ash on cement hydration and mechanical property of mortar." *Adv. Civ. Eng.* 2018: 1–7. https://doi.org/10.1155/2018/4023178.

Freiesleben Hansen, P., and E. J. Pedersen. 1985. "Curing of concrete structures." In *Draft DEB—Guide to durable concrete structures*. Lausanne, Switzerland: Comité Euro-International du Béton.

Haustein, E., and A. Kuryłowicz-Cudowska. 2020. "The effect of fly ash microspheres on the pore structure of concrete." *Minerals* 10 (1): 58. https://doi.org/10.3390/min10010058.

Jonasson, J. E., P. Groth, and H. Hedlund. 1994. "Modeling of temperature and moisture field in concrete to study early age movements as a basis for stress analysis." In *Proc., Int. Symp. Thermal Cracking in Concrete at Early Ages*, 45–52. Munich, Germany: RILEM.

Kada-Benameur, H., E. Wirquin, and B. Duthoit. 2000. "Determination of apparent activation energy of concrete by isothermal calorimetry." *Cem. Concr. Res.* 30 (2): 301–305. https://doi.org/10.1016/S0008-8846(99)00250-1.

Kim, J.-K., S. H. Han, and Y. C. Song. 2002. "Effect of temperature and aging on the mechanical properties of concrete. Part I: Experimental results." *Cem. Concr. Res.* 32 (7): 1087–1094. https://doi.org/10.1016/S0008-8846(02)00744-5.

Kjellsen, K. O., and R. J. Detwiler. 1993. "Later-age strength prediction by a modified maturity model." ACI Mater. J. 90 (3): 220–227.

Kleinhans, U., C. Wieland, F. J. Frandsen, and H. Spliethoff. 2018. "Ash formation and deposition in coal and biomass fired combustion systems: Progress and challenges in the field of ash particle sticking and rebound behavior." *Prog. Energy Combust. Sci.* 68 (Sep): 65–168. https://doi.org/10.1016/j.pecs.2018.02.001.

Klemczak, B., and M. Batog. 2016. "Heat of hydration of low-clinker cements. Part I: Semi-adiabatic and isothermal tests at different temperature." *J. Therm. Anal. Calorim.* 123 (2): 1351–1360. https://doi.org/10.1007/s10973-015-4782-y.

Kurpinska, M., B. Grzyl, M. Pszczola, and A. Kristowski. 2019. "The application of granulated expanded glass aggregate with cement grout as an alternative solution for sub-grade and frost-protection sub-base layer in road construction." *Materials* 12 (21): 3528. https://doi.org/10.3390/ma12213528.

Kurpinska, M., and L. Kułak. 2019. "Predicting performance of lightweight concrete with granulated expanded glass and ash aggregate by means of using artificial neural networks." *Materials* 12 (12): 2002. https://doi.org/10.3390/ma12122002.

Kuryłowicz-Cudowska, A. 2019. "Determination of thermophysical parameters involved in the numerical model to predict the temperature field of cast-in-place concrete bridge deck." *Materials* 12 (19): 3089. https://doi.org/10.3390/ma12193089.

Kuryłowicz-Cudowska, A., K. Wilde, and J. Chróścielewski. 2020. "Prediction of cast-in-place concrete strength of the extradosed bridge deck based on temperature monitoring and numerical simulations." *Constr. Build. Mater.* 254 (Sep): 11924. https://doi.org/10.1016/j.conbuildmat.2020.119224.

Mariak, A., J. Chróścielewski, and K. Wilde. 2017. "Numerical simulation of hardening of concrete plate." In *Proc., 11th Int. Conf. on Shell Structures: Theory and Applications*. London: Taylor and Francis Group.

Mariak, A., M. Kurpińska, and K. Wilde. 2018. “Maturity curve for estimating the in-place strength of high performance concrete.” In Vol. 262 of *Proc., MATEC Web Conf.*, 06007. Les Ulis, France: EDP Sciences. https://doi.org/10.1051/matecconf/201926206007.

Martinelli, E., E. A. B. Koenders, and A. Caggiano. 2013. “A numerical recipe for modelling hydration and heat flow in hardening concrete.” *Cem. Concr. Compos.* 40 (Jul): 48–58. https://doi.org/10.1016/j.cemconcomp.2013.04.004.

Miśkiewicz, M., D. Bruski, J. Chróścielewski, and K. Wilde. 2019. “Safety assessment of a concrete viaduct damaged by vehicle impact and an evaluation of the repair.” *Eng. Fail. Anal.* 106 (Dec): 104147. https://doi.org/10.1016/j.engfailanal.2019.104147.

Moghaddam, F., V. Sirivivatnanon, and K. Vessalas. 2019. “The effect of fly ash fineness on heat of hydration, microstructure, flow and compressive strength of blended cement pastes.” *Case Stud. Constr. Mater.* 10: e00218. https://doi.org/10.1016/j.cscm.2019.e00218.

Poole, J. L., K. A. Riding, M. C. G. Juenger, K. J. Folliard, and A. K. Schindler. 2011. “Effect of chemical admixtures on apparent activation energy of cementitious systems.” *J. Mater. Civ. Eng.* 23 (12): 1654–1661. https://doi.org/10.1061/(ASCE)MT.1943-5533.0000345.

Saadoon, T., B. G´omez-Meijide, and A. Garcia. 2019. “New predictive methodology for the apparent activation energy and strength of conventional and rapid hardening concretes.” *Cem. Concr. Res.* 115 (Jan): 264–273. https://doi.org/10.1016/j.cemconres.2018.10.020.

Schindler, A. K. 2004. “Effect of temperature on hydration of cementitious materials.” *ACI Mater. J.* 101 (1): 72–81.

Snelson, D. G., S. Wild, and M. O’Farrell. 2008. “Heat of hydration of Portland cement–metakaolin–fly ash (PC–MK–PFA) blends.” *Cem. Concr. Res.* 38 (6): 832–840. https://doi.org/10.1016/j.cemconres.2008.01.004.

Soutsos, M. N., G. Turu’allo, K. Owens, J. Kwasny, S. J. Barnett, and P. A. M. Basheer. 2013. “Maturity testing of lightweight selfcompacting and vibrated concretes.” *Constr. Build. Mater.* 47 (Oct): 118–125. https://doi.org/10.1016/j.conbuildmat.2013.04.045.

Vu, D.-H., H.-B. Bui, B. Kalantar, X.-N. Bui, D.-A. Nguyen, Q.-T. Le, N.-H. Do, and H. Nguyen. 2019. “Composition and morphology characteristics of magnetic fractions of coal fly ash wastes processed in high-temperature exposure in thermal power plants.” *Appl. Sci.* 9 (9): 1964. https://doi.org/10.3390/app9091964.

Wadsö, L. 2003. *An Experimental comparison between isothermal calorimetry, semiadiabatic calorimetry and solution calorimetry for the study of cement hydration.* Nordtest Rep. No. TR 522. Serravalle Scrivia, Italy: Nordtest.

Table 1. Chemical compositions and physical properties of the materials used

Property	CEM I 42.5 R	FA
SiO_2 (% by weight)	21.23	55.44
Fe_2O_3 ((% by weight)	2.23	6.36
Al_2O_3 ((% by weight)	4.99	24.57
CaO ((% by weight)	64.08	3.65
MgO ((% by weight)	2.48	2.57
SO_3 ((% by weight)	2.97	0.62
Na_2O ((% by weight)	0.13	1.04
K_2O ((% by weight)	0.92	3.04
Chloride content ((% by weight)	0.04	–
LOI ((% by weight)	2.96	2.56
Density (g/cm^3)	3.05	2.10
Specific surface area (cm^2/g)	2.360	2.250

Note: LOI = loss on ignition.

Table 2. Chemical composition of natural pozzolans (N) and FA (F, C) according to ASTM C618

Chemical requirements	Class (%)		
	N	F	C
$SiO_2 + Al_2O_3 + Fe_2O_3$, min.	70.0	70.0	50.0
SO_3, max.	4.0	5.0	5.0
Humidity, max.	3.0	3.0	3.0
LOI, max.	10.0	6.0	6.0

Source: Data from ASTM (2019b)
Note: N = natural pozzolans; F = fly ash Class F; C = fly ash Class C; and LOI = loss on ignition.

Table 3. Computation results for the coefficients a and b of Eq. (4)

Mortar mixture identifier	Curing temperature (°C)	Constant		
		a	b	R^2
OPC	23	351.8	–18.68	0.9979
	33	346.6	–9.40	0.9991
	43	353.8	–6.10	0.9892
	53	362.6	–4.58	0.9827
OPC + 10% FA	23	321.7	–22.03	0.9992
	33	319.8	–11.53	0.9994
	43	320.5	–6.46	0.9895
	53	331.1	–6.61	0.9943
OPC + 20% FA	23	302.6	–24.51	0.9994
	33	316.4	–12.93	0.9996
	43	319.5	–9.17	0.9856
	53	336.3	–8.95	0.9959

Table 4. Characteristic values for the considered mortars

Mortar mixture identifier	Curing temperature (°C)	Parameter			
		Q_{tot} (J/g)	$\dot{Q}_{peak\_1}$ [J/(g·h)]	$\alpha\ (\dot{Q}_{peak\_1})$	$t\ (\dot{Q}_{peak\_1})$ (h)
OPC	23	351.8	8.45	0.22	10.5
	33	346.6	14.22	0.22	6.6
	43	353.8	27.37	0.22	4.5
	53	362.6	38.06	0.24	3.5
OPC + 10% FA	23	321.7	7.80	0.18	10.8
	33	319.8	12.11	0.19	6.9
	43	320.5	24.94	0.20	4.6
	53	331.1	33.53	0.19	3.7
OPC + 20% FA	23	302.6	7.00	0.18	11.3
	33	316.4	11.49	0.21	7.0
	43	319.5	21.05	0.20	5.1
	53	336.3	30.00	0.20	4.0

Table 5. Analysis results for E_a obtained using the hyperbolic function

Mortar mixture identifier	Curing temperature (°C)	Nonlinear fit				Straight-line fit	
		S_u (MPa)	k (day^{-1})	t_0 (day)	R^2	E_a (kJ/mol)	R^2
OPC	23	64.15	1.172	0.423	0.9980	**41.077**	**0.9562**
	33	53.34	1.446	0.198	0.9974		
	43	53.01	3.137	0.153	0.9948		
	53	40.47	4.879	0.080	0.9708		
OPC + 10% FA	23	57.97	1.050	0.416	0.9914	**35.020**	**0.9998**
	33	53.60	1.700	0.219	0.9507		
	43	51.52	2.600	0.151	0.9843		
	53	44.70	3.902	0.061	0.9196		
OPC + 20% FA	23	53.59	0.647	0.387	0.9872	**33.975**	**0.9778**
	33	51.83	1.129	0.162	0.9969		
	43	56.08	1.426	0.122	0.9892		
	53	48.81	2.456	0.053	0.9617		

Note: Bold values indicate the main results of calculations.

Table 6. Analysis results for E_a obtained using the exponential function

Mortar mixture identifier	Curing temperature (°C)	Nonlinear fit				Straight-line fit	
		S_u (MPa)	$k = 1/\tau$ (day^{-1})	β	R^2	E_a (kJ/mol)	R^2
OPC	23	61.60	1.068	1.271	0.9949	**44.011**	**0.9964**
	33	52.72	1.737	1.056	0.9965		
	43	53.20	3.183	1.085	0.9931		
	53	44.27	5.447	0.622	0.9943		
OPC + 10% FA	23	56.50	1.031	1.149	0.9836	**39.986**	**0.9514**
	33	58.19	1.262	0.747	0.9861		
	43	53.40	2.476	0.896	0.9819		
	53	49.03	4.376	0.580	0.9783		
OPC + 20% FA	23	56.41	0.711	0.842	0.9844	**37.686**	**0.9956**
	33	54.12	1.071	0.901	0.9757		
	43	59.77	1.799	0.719	0.9937		
	53	58.54	2.870	0.492	0.9886		

Note: Bold values indicate the main results of calculations.

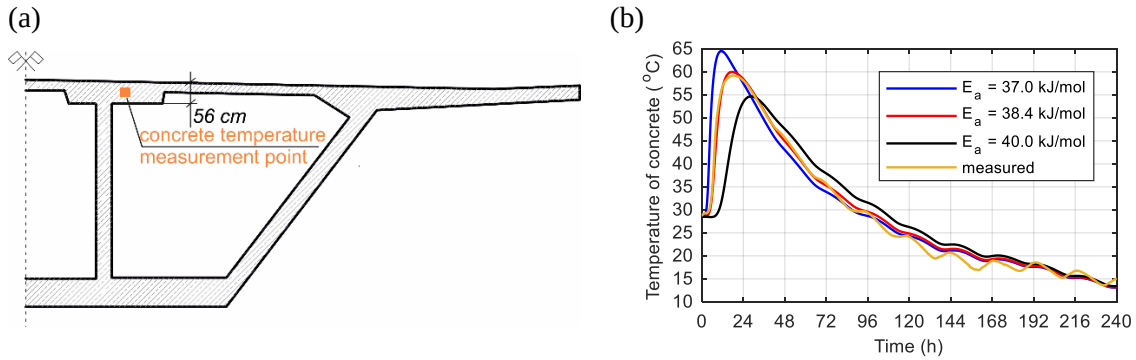

Fig. 1. (a) Half of the cross section of the bridge span; (b) concrete temperature distribution for different values of the apparent activation energy.

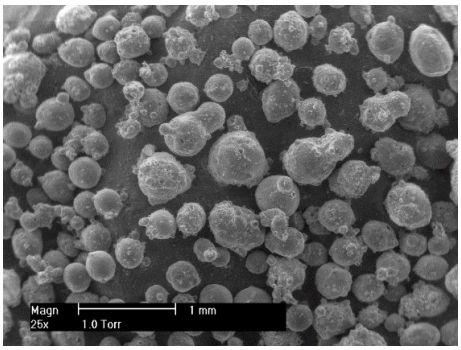

Fig. 2. Microscope image of the siliceous FA grain structure (magnification of 25 times).

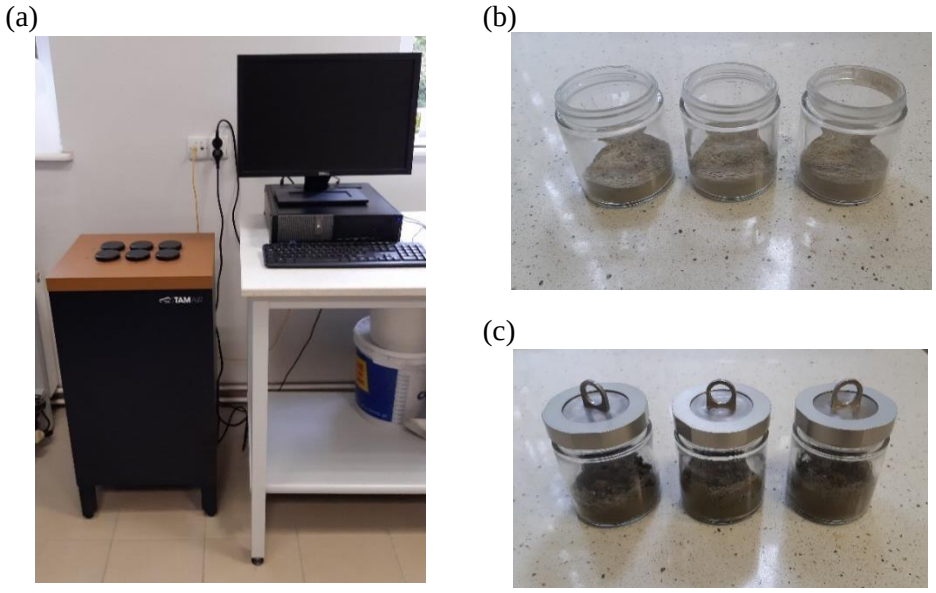

Fig. 3. (a) Isothermal calorimeter; and (b and c) mortar specimens in glass ampoules.

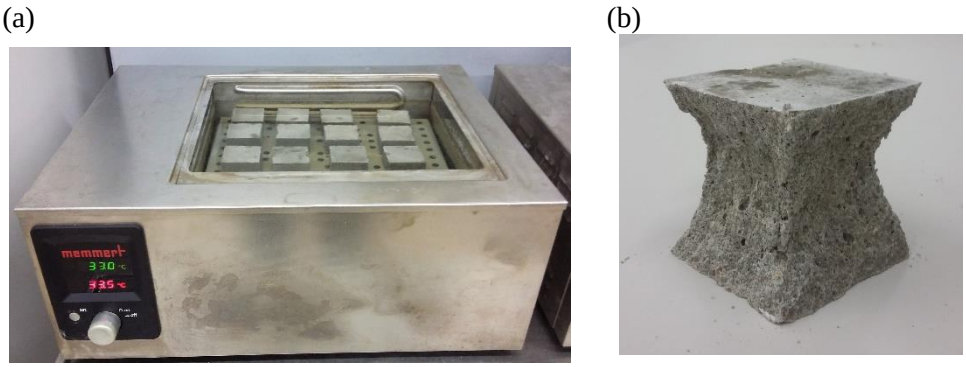

Fig. 4. (a) Mortar cubes in the water bath at 33 °C; and (b) mortar cube after the compression test.

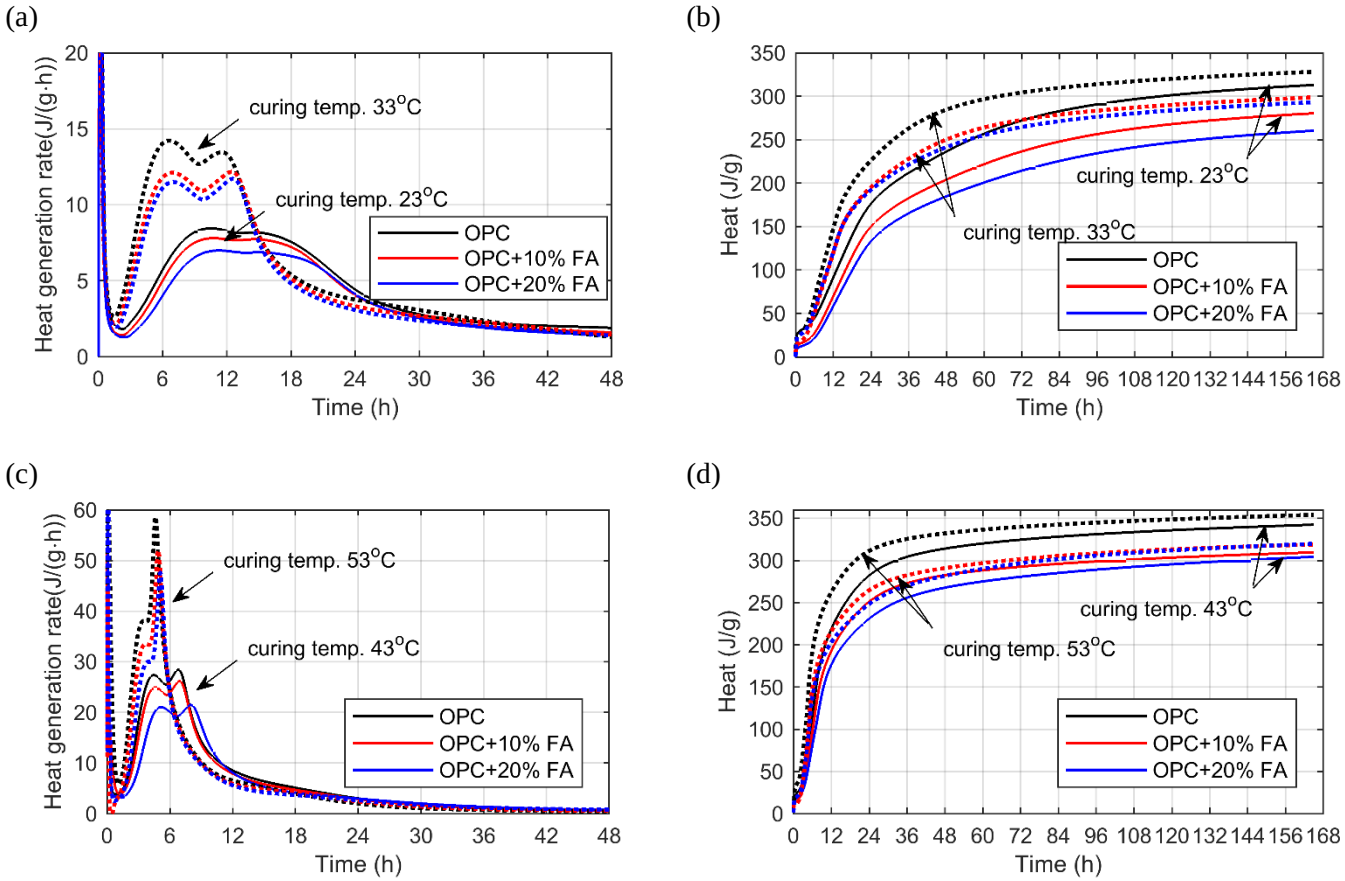

Fig. 5. Effects of FA addition on the heat generation rate and heat of hydration of mortars cured at different temperatures: (a and b) 23°C and 33°C; and (c and d) 43°C and 53°C.

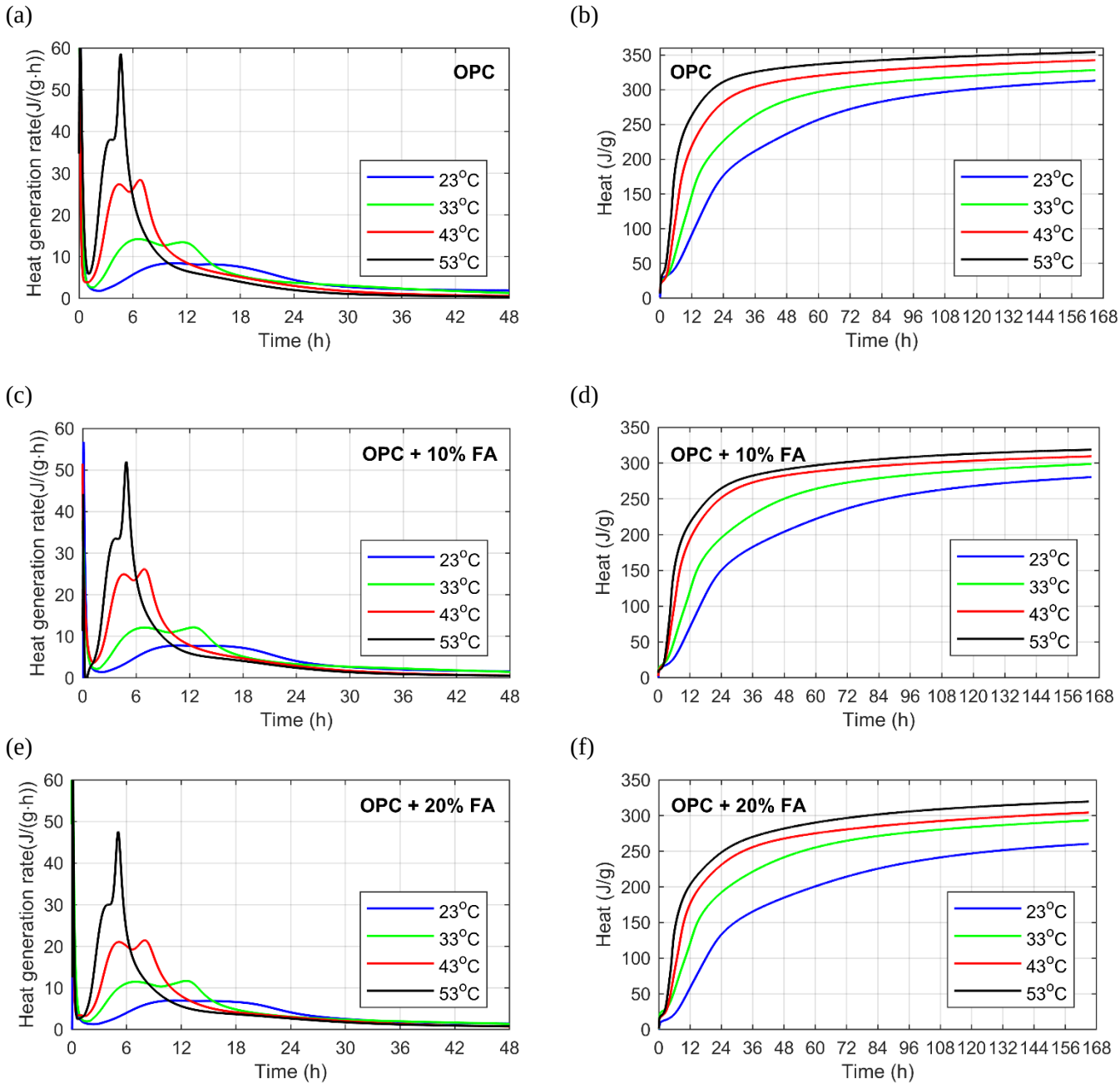

Fig. 6. Effects of the curing temperature on the heat generation rate and heat of hydration of mortars: (a and b) OPC; (c and d) OPC + 10% FA; and (e and f) OPC + 20% FA.

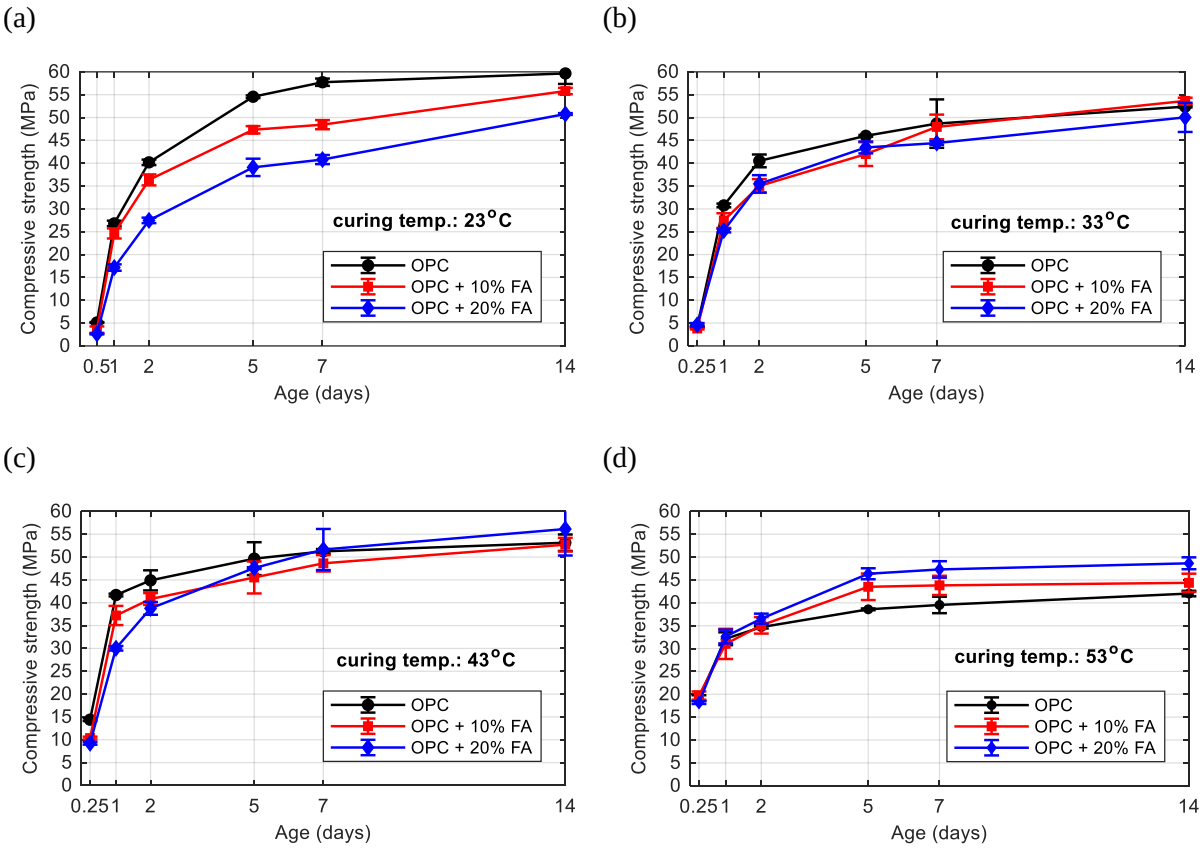

Fig. 7. Average compressive strength of mortar specimens cured at different temperatures: (a) 23°C; (b) 33°C; (c) 4 °C; and (d) 53 °C.

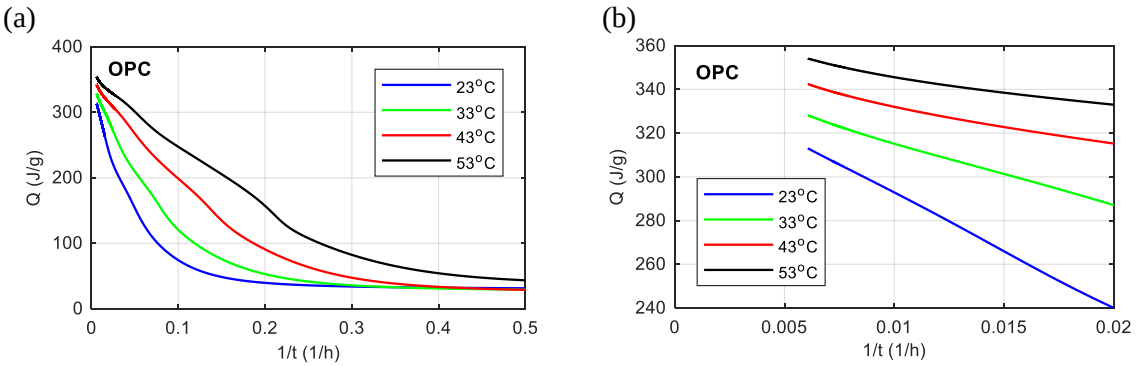

Fig. 8. Extrapolation procedure of Q_{tot} for the OPC mortar mixture: (a) $1/t < 0.5$; and (b) $1/t < 0.02$.

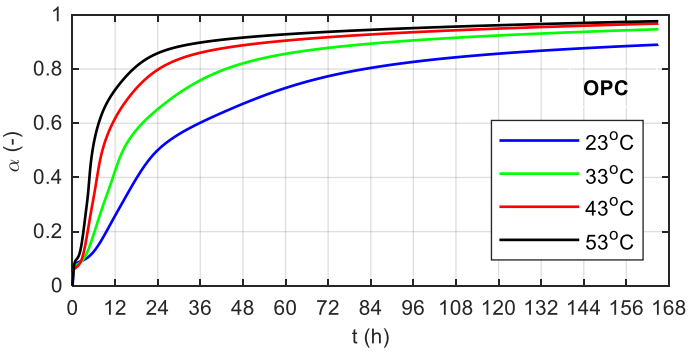

Fig. 9. Degree of heat development α versus time t for mortar with OPC.

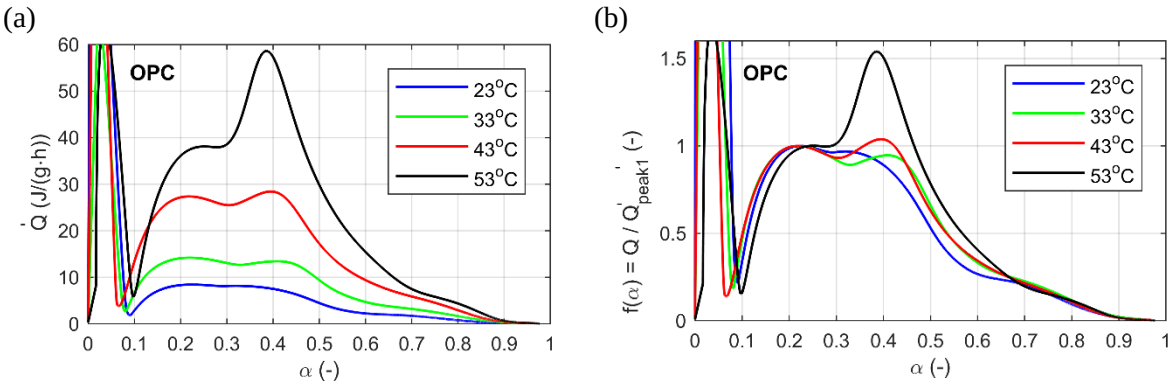

Fig. 10. Analysis of mortar with OPC: (a) heat generation rate $\dot{Q}$ with respect to α; and (b) normalized heat generation rate $f(\alpha)$ according to $\dot{Q}_{peak\_1}$.

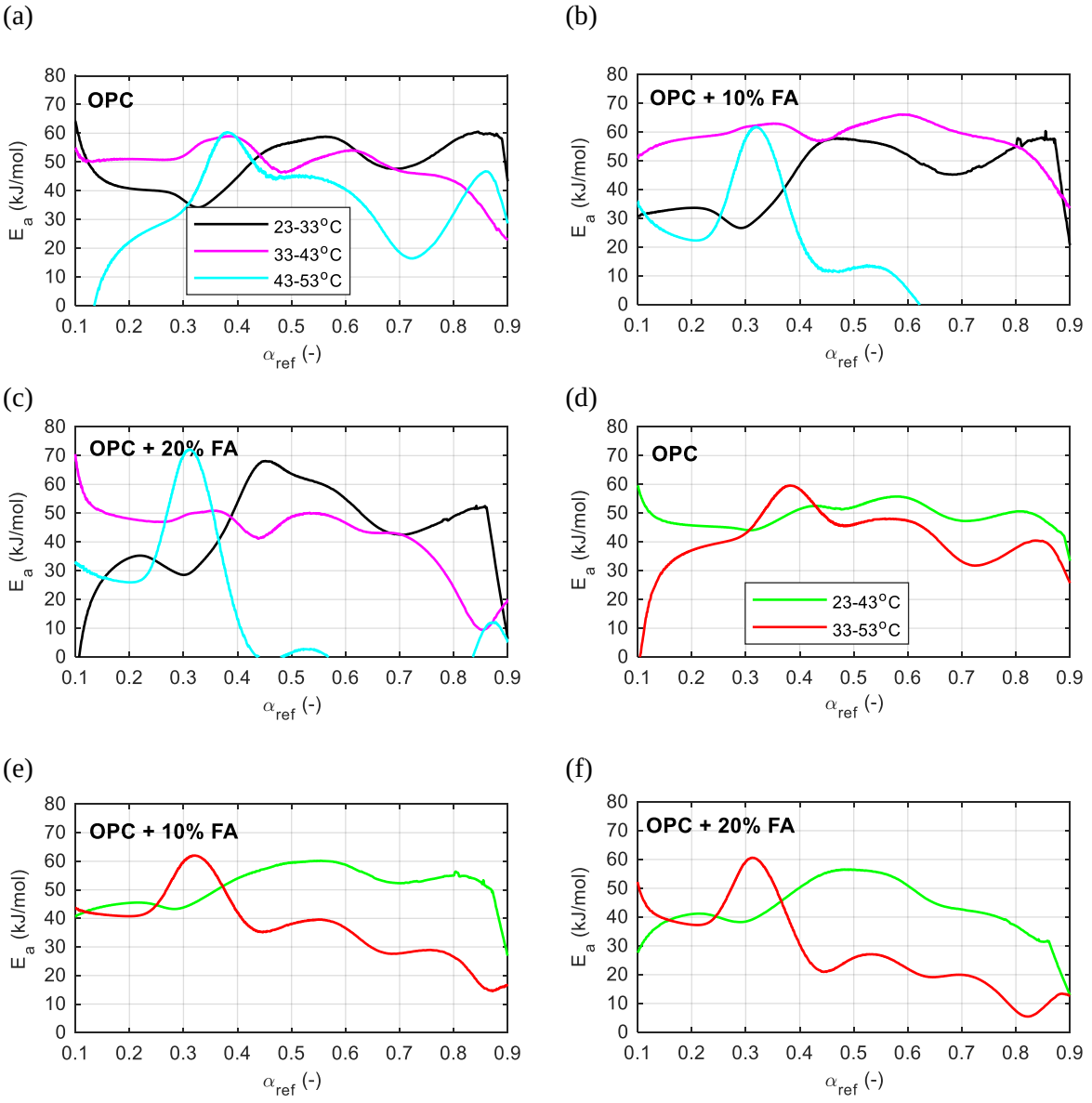

Fig. 11. Evolution of the activation energy for the considered mortars: (a–c) three temperature intervals; and (d–f) two temperature intervals.

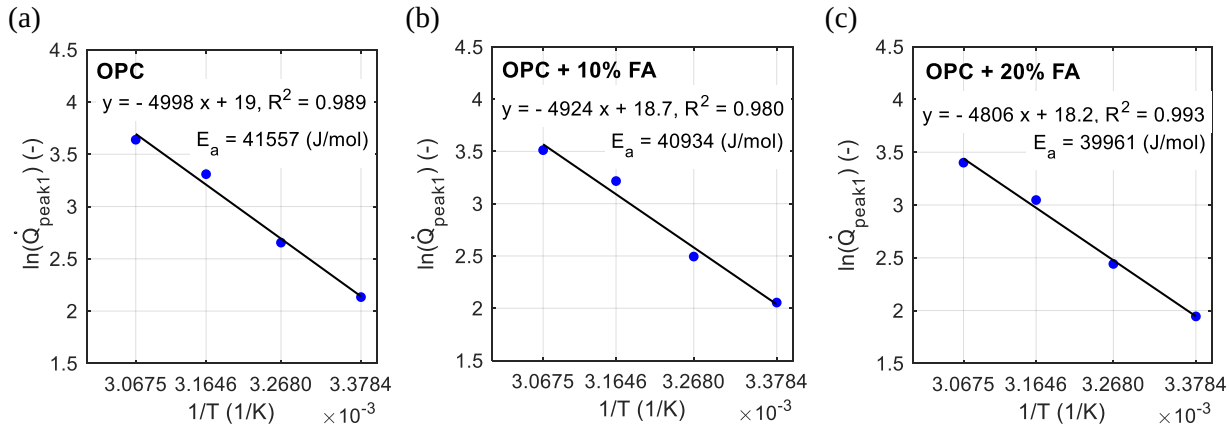

Fig. 12. Activation energy for three mortar mixtures based on $\ln(\dot{Q}_{peak\_1})$: (a) mortar with OPC; (b) mortar with OPC + 10% FA; and (c) mortar with OPC + 20% FA.

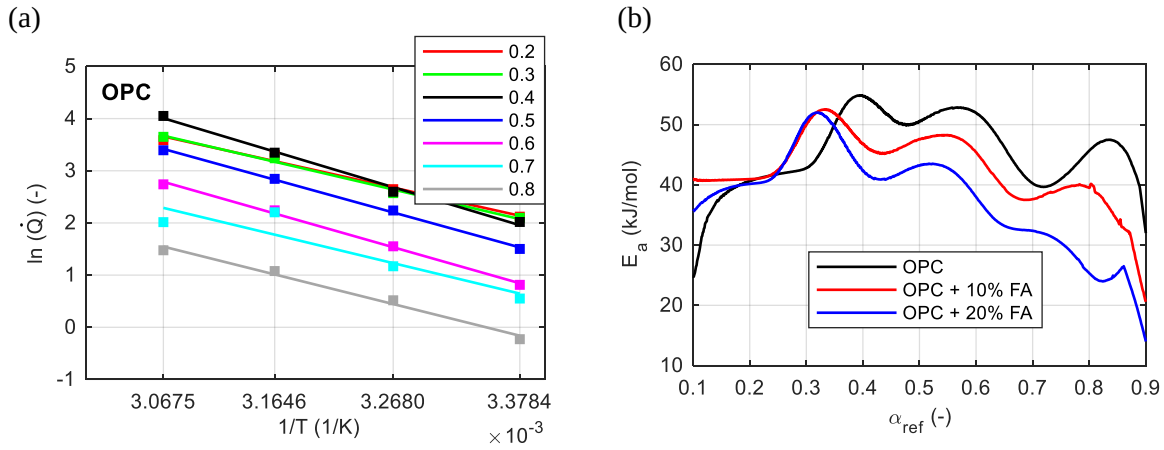

Fig. 13. (a) Linear fit of $\ln(\dot{Q})$ for selected values of α ; and (b) apparent activation energy for the three mortar mixtures, determined using the logarithmic formulation.

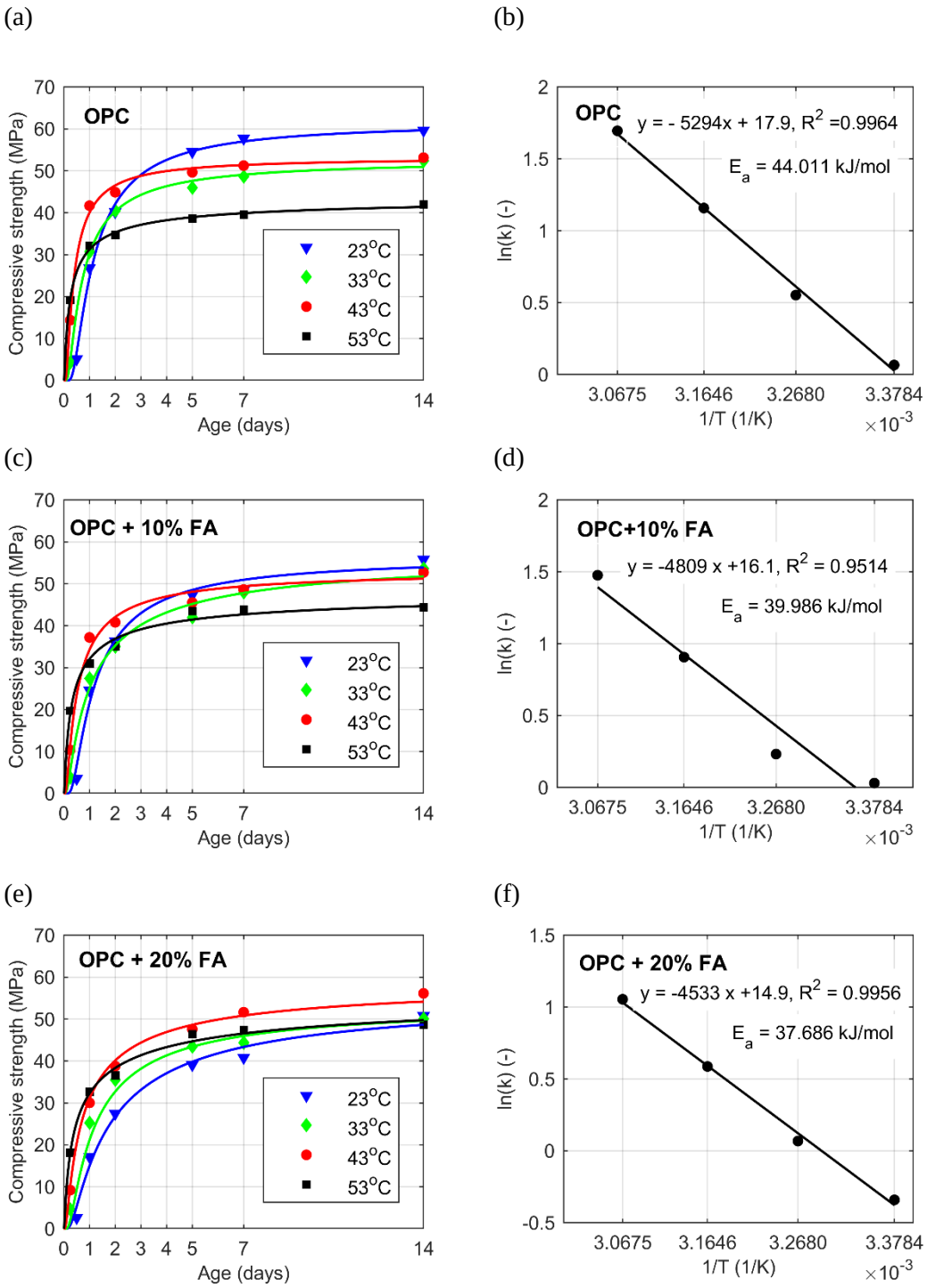

Fig. 14. Strength–age curves approximated using the exponential function and the appropriate activation energy: (a and b) OPC; (c and d) OPC + 10% FA; and (e and f) OPC + 20% FA.

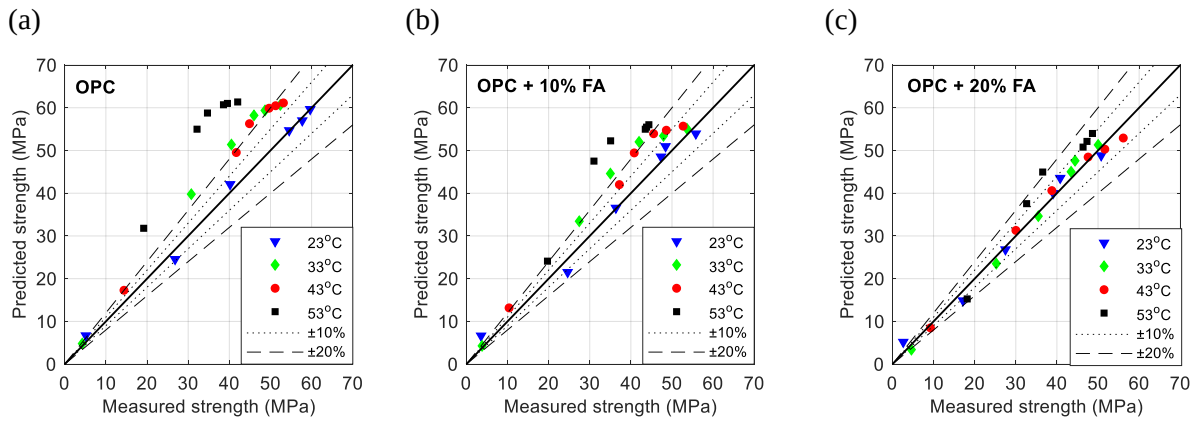

Fig. 15. Measured strength versus the strength estimated via the maturity method using the exponential function for different mixtures: (a) OPC; (b) OPC + 10% FA; and (c) OPC + 20% FA.